Journal of Inflammation Research

Dovepress
Taylor & Francis Group

Open Access Full Text Article

ORIGINAL RESEARCH

Abnormal Alterations in EEG Microstates and Functional Networks in Anti-LGI1 Antibody Encephalitis

Lei Wang[1,*], Ping Jiang[1,*], Yingfan Wang[1,*], Dingfeng Sun[1], Ailiang Miao[1,2], Xiaoshan Wang[1]

[1]Department of Neurology, The Affiliated Brain Hospital of Nanjing Medical University, Nanjing Medical University, Nanjing, Jiangsu, People's Republic of China; [2]Department of Video-Electroencephalogram, The Affiliated Brain Hospital of Nanjing Medical University, Nanjing, Jiangsu, People's Republic of China

*These authors contributed equally to this work

Correspondence: Xiaoshan Wang; Ailiang Miao, Email lidou2005@126.com; ailiangmiao1986@163.com

Objective: This study aimed to use electroencephalogram (EEG) microstate analysis to characterize transient topographic patterns and rapid brain network reorganization in anti-leucine-rich glioma-inactivated 1 (LGI1) antibody encephalitis (anti-LGI1-AE).

Methods: EEG data were collected from fifteen patients with anti-LGI1-AE and eighteen age- and sex-matched controls. K-means clustering was used to extract microstate sequences, and temporal parameters were compared between groups. For microstates showing significant differences, weighted phase lag index matrices were computed across frequency bands, and network-based statistics were applied to identify functional connectivity differences.

Results: The topographic pattern of Microstate A differed significantly between the anti-LGI1-AE group and the control group (p = 0.002). Patients exhibited a significantly higher occurrence of Microstates B and C (p = 0.015 and p = 0.001, respectively). Additionally, the mean global field power of Microstate C was reduced in the patient group (p = 0.007). The transition probability from Microstate A to B was increased in patients (p = 0.013), though this difference did not remain significant after false discovery rate (FDR) correction ($pFDR$ = 0.161). EEG functional network analysis based on microstates with significant differences revealed that, during Microstate B, patients showed a widespread increase in whole-brain functional connectivity in the beta frequency band (all $p < 0.001$). During Microstate C, enhanced delta-band connectivity was observed with the left occipital region serving as a core hub (p = 0.002). Beta-band connectivity was also increased between the left posterior temporal region, midline structures, and left parietal regions (p = 0.037).

Conclusion: Widespread alterations in functional brain networks are present in anti-LGI1-AE. Changes in microstate temporal parameters and enhanced functional connectivity may reflect compensatory regulatory mechanisms or pathological hyperactivation, revealing functional brain changes that go beyond overt structural damage.

Keywords: anti-LGI1 antibody encephalitis, anti-LGI1-AE, electroencephalography, EEG, microstate, functional brain connectivity, weighted phase lag index, WPLI

Introduction

Anti-leucine-rich glioma-inactivated 1 (LGI1) antibody encephalitis (anti-LGI1-AE) is one of the most common forms of limbic encephalitis, mediated by antibodies targeting LGI1—a synaptic protein enriched in leucine-rich repeats. Clinical heterogeneity and a high rate of negative findings in routine examinations often lead to delayed diagnosis. The most characteristic manifestation is faciobrachial dystonic seizures (FBDS), characterised by brief, unilateral jerks affecting the face and/or ipsilateral limbs.[1] Despite growing recognition among neurologists, Flanagan et al reported that a substantial proportion of patients receive initial misdiagnoses of psychiatric or functional disorders, with 19% suspected of Creutzfeldt–Jakob disease.[2] Some seizure semiology may mimic panic attacks or anxiety episodes.[1] Approximately half of patients develop neuropsychiatric symptoms, including depression, anxiety, paranoia,

Received: 30 May 2025
Accepted: 27 October 2025
Published: 12 November 2025

hallucinations, and emotional lability (eg, pathological crying).[1,3,4] Cognitive deficits extend beyond mixed anterograde-retrograde amnesia[5] to include impairments in attention, verbal fluency, and executive function.[3,6,7] Electroencephalographic (EEG) abnormalities are common, with nearly half of cases showing non-specific background rhythm irregularities.[8] Furthermore, a negative magnetic resonance imaging (MRI) in anti-LGI1-AE is frequent,[9,10] and cerebrospinal fluid (CSF) findings often lack typical inflammatory changes,[10,11] increasing the likelihood of misdiagnosis.

^{18}F-fluoro-2-deoxy-*d*-glucose positron emission tomography studies have revealed metabolic abnormalities in regions such as the basal ganglia, prefrontal cortex, anterior cingulate cortex, parietal cortex, brainstem, and cerebellum.[12,13] Functional magnetic resonance imaging (fMRI) has demonstrated significantly increased connectivity within the dorsal and ventral default mode networks (DMN), higher-order visual networks, and sensorimotor networks, along with decreased connectivity in the salience network.[14] However, the limited temporal resolution of these imaging modalities makes it difficult to capture transient neural processes. In contrast, EEG, as a non-invasive and cost-effective imaging technique, enables the detection of neural dynamics at the millisecond scale, offering a more detailed and temporally precise perspective on brain function.

EEG microstates were first identified by Lehmann et al[15] and refer to brief periods during which the scalp voltage topography remains quasi-stable These microstates are typically extracted at peaks of the global field power (GFP) and are thought to represent transient, global configurations of brain functional activity. In resting-state EEG, the majority (>70%) of the data can be explained by just four canonical topographic classes, traditionally labeled as Microstates A, B, C, and D.[16] Transitions between microstates do not occur gradually but rather switch abruptly, typically after maintaining a dominant configuration for approximately 80–120 milliseconds.[17] The sequence of transitions between microstates forms a temporal structure that is considered to reflect dynamic changes in brain network activity. The temporal properties of EEG microstate sequences can be modulated by various internal and external stimuli, including global brain states,[18] spontaneous thought processes,[19] behavioral tasks,[20] and pharmacological interventions.[21] Altered microstate dynamics have been reported in patients with schizophrenia,[22] Alzheimer's disease,[22] stroke,[23] and temporal lobe epilepsy,[24] demonstrating significant deviations from patterns observed in healthy individuals. To date, however, the EEG microstate characteristics in patients with anti-LGI1-AE remain unexplored.

Materials and Methods

Participants

Anti-LGI1-AE Group

Patients diagnosed with anti-LGI1-AE at Nanjing Brain Hospital between 2019 and 2024 were enrolled in the study. All patients met the diagnostic criteria for autoimmune encephalitis as outlined in the 2016 *Lancet Neurology* consensus guidelines.[10] Inclusion criteria were as follows:

1. Acute (less than 6 weeks) or subacute (more than 6 weeks but less than 3 months) onset of symptoms, including seizures, cognitive impairment, psychiatric manifestations, or FBDS;
2. Positive anti-LGI1 antibodies detected in CSF or serum via cell-based assay;
3. Elevated CSF white cell count (>5 × 10^6/L), with lymphocytic pleocytosis or positive oligoclonal bands on CSF cytological analysis;
4. MRI evidence of T2-weighted or FLAIR hyperintensities involving limbic system structures.

Exclusion Criteria:

1. Exclusion of other neurological disorders that could account for similar clinical manifestations, such as infectious encephalitis, other antibody-associated encephalitides, or metabolic encephalopathies;
2. A history of other neurological or psychiatric disorders prior to the onset of autoimmune encephalitis.

Control Group

The control group consisted of individuals who presented with mild neurological symptoms (eg, headache or mild anxiety). Participants were matched to the anti-LGI1-AE group by sex and gender. None of the control subjects had a history of, or clinical symptoms consistent with, anti-LGI1-AE. Additionally, they had not taken any medications that could affect EEG signals, such as antiepileptic drugs, antipsychotics, or antidepressants. All participants underwent MRI scans to rule out structural brain abnormalities.

EEG Recording

EEG recordings were conducted in a controlled environment with constant lighting and background noise from air conditioning. Prior to the recording, participants were thoroughly informed about the experimental procedures and safety measures. They were instructed to minimize muscle activity and eye movements to reduce recording artifacts. During the session, participants lay on a bed, kept their eyes closed, remained relaxed, and were asked to stay awake. Continuous 10-minute EEG data were collected during the eyes-closed, awake resting state. Following the recording, EEG data and symptom reports provided by family members were analyzed by physicians specializing in the clinical management and EEG interpretation of autoimmune encephalitis.

EEG data were recorded by certified technicians using the Nicolet System One device (CareFusion, San Diego, CA) at a sampling rate of 256 Hz. Electrodes were placed according to the international 10–20 system. Transparent conductive gel was applied to the scalp to reduce electrode impedance, which was maintained below 5 kΩ throughout the recording.

Preprocessing

EEG signals were preprocessed by removing DC drifts, applying a 2–20 Hz band-pass filter, and re-referencing the data to the average reference. The continuous EEG data were segmented into epochs of 6 seconds each.[25] During the quality control phase, both manual visual inspection and automated artifact detection algorithms were employed to identify and handle abnormal signals. Specifically, bad channels were detected based on multiple criteria, including extreme amplitudes, abnormal voltage distributions, excessive drifts, abnormal kurtosis, and muscle activity. The following protocol was applied: up to 20% of electrodes could be rejected. If the number of bad electrodes exceeded this threshold, they were ranked by the frequency of extreme artifacts across segments, and only the top 20% were removed. A similar approach was used for epoch rejection, where segments containing extreme artifacts were marked and discarded to ensure data quality. After artifact removal, signals were re-referenced, and spherical spline interpolation was used to reconstruct the signals of removed electrodes. Independent Component Analysis (ICA) using the Picard algorithm[26] was then applied to identify components associated with artifacts. These components were classified and rejected using the ICLabel module embedded in the Brainstorm toolbox,[27] yielding clean neural signals. Finally, a continuous 5-minute segment of EEG data was obtained for subsequent microstate analysis. For more information on Brainstorm, refer to the official website: https://neuroimage.usc.edu/brainstorm/.

Microstate Analysis

Microstate analysis was conducted using the Cartool software and involved three key steps. Detailed procedures can be found in the official tutorial: https://github.com/gaffreylab/EEG-Microstate-Analysis-TutorialWiki.

Stage 1: Individual-Level Clustering

EEG topographic maps were extracted at peaks of GFP, as these points exhibit the highest signal strength and signal-to-noise ratio, thereby improving the accuracy of subsequent k-means clustering.[28] Specifically, 50 epochs were randomly selected from each participant's continuous 5-minute EEG recording. These epochs were then subjected to polarity-invariant modified k-means clustering, repeated 50 times, to identify 1–12 topographic clusters per epoch. This resampling strategy was adopted to enhance the reliability of clustering outcomes.[29,30] To determine the optimal number of clusters for each epoch, a meta-criterion approach was used. This method integrates six independent clustering validity indices to ensure robust and consistent model selection.[31]

Stage 2: Group-Level Clustering

First, the optimal k clusters from each participant's 50 epochs were pooled together. From this combined dataset, 100 new epochs were randomly sampled, each representing 99.9% of the group-level topographic variability. These epochs were then subjected to polarity-invariant modified k-means clustering, repeated 100 times, with the number of clusters set from 1 to 15. To determine the optimal number of clusters, the meta-criterion was again applied to each epoch. The resulting topographic maps were merged and underwent a final round of k-means clustering using the same parameters. The final group-level microstate maps were selected based on both the meta-criterion results and the topographic patterns typically observed in resting-state studies. If the meta-criterion curve presented a clear single peak, that solution was chosen. However, in cases where multiple local maxima were observed, researchers used expert judgment to determine the most appropriate solution rather than selecting the one with the absolute highest score.[32] All microstate topographies were visualized using MATLAB (https://ww2.mathworks.cn/products/matlab.html).

Stage 3: Backfitting

Back-fitting was performed on each participant's preprocessed and spatially filtered data to match the group-level microstates with individual data in the time dimension, thereby identifying which group microstate each participant belonged to at each time point. First, each participant's data was normalized by the median GFP to minimize amplitude differences across individuals. This prevents high-amplitude signals from dominating and low-amplitude signals from being underestimated during microstate template backfitting. The median was chosen over the mean because it is less sensitive to outliers, ensuring more robust normalization. Then, each time point was assigned to the group microstate with the most similar topography using spatial correlation, with the minimum correlation for time-point assignment set to 0.50, regardless of polarity. After the assignment, temporal smoothing was applied with a half-window width of 32 ms and a Besag factor of 10[33]. Illogical short segments were discarded: segments shorter than 32 ms were split into two parts, with the first half merged into the preceding segment and the second half merged into the following segment. Finally, for each microstate, the following metrics were calculated for each participant: Mean GFP, Mean Duration, Time Coverage, and Segment Count Density. Additionally, transition probabilities were computed based on a first-order Markov chain model (including expected and observed values). To account for individual differences in microstate occurrence frequency, the observed probabilities for each transition were normalized by dividing them by the corresponding expected probabilities.

Brain Network Construction

Brain networks were constructed for microstates with significant differences in time parameters to further analyze the brain functional connectivity characteristics in patients with anti-LGI1-AE: 1) Node Selection: All scalp electrodes were selected as the nodes corresponding to the brain functional network. 2) Association Matrix Calculation: The EEG signals from 2–20 Hz were divided into four main frequency bands: delta (2–4 Hz), theta (4–8 Hz), alpha (8–12 Hz), and beta (12–20 Hz). The Weighted Phase Lag Index (WPLI) algorithm was used to calculate the phase synchronization between each pair of nodes, resulting in a 19×19 functional connectivity matrix. WPLI effectively quantifies the phase coupling strength between two signals and avoids the sensitivity to volume conduction effects that traditional coherence measures may have.[34] In the WPLI calculation, the EEG signals were first transformed using Fourier analysis, converting the raw time-domain signals into frequency-domain signals, thereby obtaining amplitude and phase information for each frequency point. Next, the phase difference between any two signals at a specific frequency was calculated. The sign function was then applied to the phase differences at each time point to extract their positive and negative directions, representing the direction of phase leading or lagging at that moment. Finally, the WPLI value was computed using the following formula: $WPLI(f) = \frac{1}{N}\sum_{n=1}^{N}|\mathrm{sign}(\Delta\phi(\mathrm{tn},f))|$, where N represents the number of phase differences involved in the calculation, and $\mathrm{sign}(\Delta\phi(\mathrm{tn},f))$ represents the direction (positive or negative) of the phase difference at each time point.

Statistical Analysis

Data analysis was conducted using SPSS 26. First, the Shapiro–Wilk test was used to determine whether the data followed a normal distribution. For normally distributed continuous variables, the data were expressed as "mean ± standard deviation" and group comparisons were performed using a *t*-test. For non-normally distributed continuous variables, the data were expressed as "median (interquartile range)" and group comparisons were performed using the Mann–Whitney *U*-test. Categorical data were expressed as "frequency (percentage)". In the brain network analysis, Network-Based Statistic (NBS) methods were used to compare functional connectivity differences between the two groups in different EEG frequency bands (delta, theta, alpha, and beta). A permutation test (5000 permutations) was conducted to control for multiple comparison errors, with a significance threshold of $p < 0.05$ after Family-Wise Error Rate (FWER) correction.[35] The difference network was visualized using BrainNet Viewer (https://www.nitrc.org/projects/bnv).[36] Group differences in topographic maps were analyzed using TANOVA in Cartool, and group comparisons of microstate transition probabilities were corrected for multiple comparisons using the False Discovery Rate (FDR) method. A corrected $p < 0.05$ was considered statistically significant.

Results

Demographic Characteristics and Clinical Manifestations

This study included 15 patients with anti-LGI1-AE (6 males, 9 females) and 18 control subjects (10 males, 8 females). The median age of the patient group was 59 years (interquartile range: 54–64 years; range: 18–68 years), and the median age of the control group was 50 years (interquartile range: 31.5–70 years; range: 17–78 years). Statistical analysis revealed no significant differences between the two groups in terms of age and gender distribution.

Seizures occurred in 11 patients (73.33%), including bilateral tonic-clonic seizures in 10 (66.67%), focal impaired awareness seizures in 2 (13.33%), and focal aware seizures in 1 (6.67%). FBDS were observed in 2 patients (13.33%). Memory impairment was present in 7 patients (46.67%), and psychiatric disorders were reported in 10 (66.67%).

EEG Characteristics

All patients with anti-LGI1 encephalitis were in the acute or subacute phase and underwent 24-hour EEG monitoring. Throughout the recording, all patients maintained normal levels of consciousness. The results indicated background abnormalities in all patients, predominantly characterised by increased slow-wave activity. The specific distributions of these abnormalities were as follows: borderline EEG findings in 2 patients (13.33%), mild generalised abnormalities in 5 (33.33%), mild focal abnormalities in 2 (13.33%), moderate generalised abnormalities in 4 (26.67%), moderate focal abnormalities in 1 (6.67%), and severe generalised abnormalities in 1 patient (6.67%). Clinical events were recorded in 5 patients (33.33%): focal seizures in 3 (20.00%), focal to bilateral tonic-clonic seizures in 1 (6.67%), bilateral tonic-clonic seizures in 1 (6.67%), and FBDS in 1 (6.67%).

EEG Microstate Analysis

Group Differences in Microstate Topographic Maps

Both the anti-LGI1-AE group and the control group identified the typical four microstates (A-D, Figure 1), with global explained variance (GEV) of 0.72 and 0.75, respectively, indicating good clustering quality in both groups. TANOVA analysis revealed a significant difference in the topographic map distribution of Microstate A between the two groups ($p = 0.002$).

Differences in Microstate Time Parameters Between Groups

There were significant differences in the microstate time parameters between the anti-LGI1-AE group and the control group. The frequency of Microstate B occurrence in the patient group was 2.40 times/second (vs control group 1.92 times/second, $p = 0.015$), and the frequency of Microstate C occurrence was 2.98 times/second (vs control group 2.12 times/second, $p = 0.001$). Additionally, the Mean GFP of Microstate C was significantly lower in the patient group ($p = 0.007$). No statistical differences were observed between the two groups in terms of average duration and time coverage for each microstate (all $p > 0.05$). Detailed data are shown in Table 1.

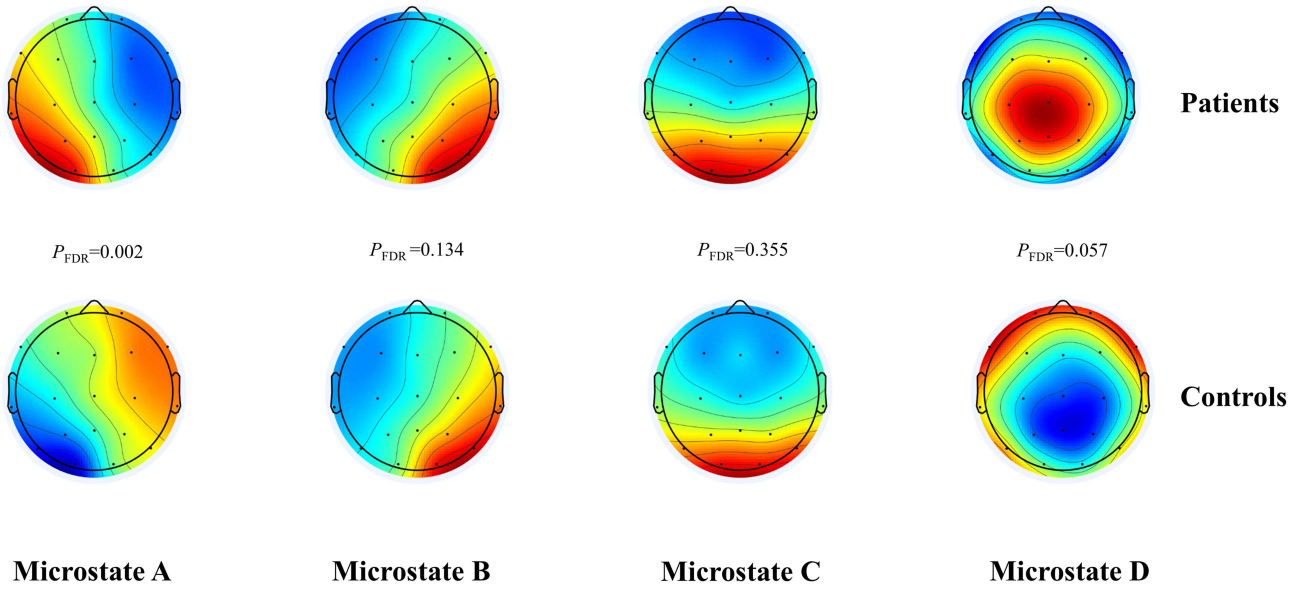

Figure 1 Comparison of differences between microstate topographies between groups.

Microstate Transition Probabilities

The transition probability from Microstate A to Microstate B was significantly higher in the anti-LGI1-AE group compared to the control group (p = 0.013). However, after FDR correction, this difference was no longer significant (FDR-corrected p = 0.161), likely reflecting limited statistical power due to the relatively small sample size. No

Table 1 Comparison of Microstate Time Parameters Between the Anti-LGI1-AE Group and the Control Group

	Anti-LGI1-AE	Controls	t	p
MeanGFP (μV)				
Microstate A	1.25±0.76	1.26±0.08	−0.481	0.634
Microstate B	1.30±0.07	1.28±0.08	1.144	0.262
Microstate C	1.37±0.07	1.50±0.18	−2.964	**0.007**
Microstate D	1.19±0.07	1.24±0.14	−1.318	0.199
MeanDur (ms)				
Microstate A	81.87±9.79	83.09±7.32	−0.400	0.693
Microstate B	84.41±9.26	83.15±8.48	0.404	0.689
Microstate C	103.50±20.94	115.24±31.01	−1.292	0.206
Microstate D	74.65±8.50	79.53±7.51	−1.730	0.095
TimeCov (%)				
Microstate A	21.58±8.41	20.56±5.83	0.396	0.696
Microstate B	24.19±7.62	19.63±5.30	1.958	0.062
Microstate C	38.95±10.71	42.07±14.44	−0.712	0.482
Microstate D	15.28±8.80	17.74±9.45	−0.773	0.446
SegDensity (seg/s)				
Microstate A	2.20±0.61	2.10±0.48	0.532	0.599
Microstate B	2.40±0.45	2.01±0.42	2.575	**0.015**
Microstate C	2.98±0.24	2.65±0.31	3.494	**0.001**
Microstate D	1.71±0.71	1.84±0.82	−0.497	0.623

Notes: Bold, p<0.05.

Abbreviations: Anti-LGI1-AE, anti-leucine-rich glioma-inactivated 1 antibody encephalitis; MeanGFP, mean global field power; MeanDur, mean duration; TimeCov, time coverage; SegDensity, segment count density.

Table 2 Comparison of Microstate Transition Probabilities Between the Anti-LGI1-AE Group and the Control Group

Transition	Anti-LGI1-AE	Controls	t	p
A to B	0.98±0.10	0.88±0.12	2.622	**0.013**
A to C	1.13±0.10	1.15±0.11	−0.712	0.482
A to D	0.81±0.10	0.87±0.13	−1.595	0.121
B to A	0.96±0.14	0.92±0.12	0.903	0.373
B to C	1.11±0.11	1.12±0.12	−0.452	0.654
B to D	0.84±0.12	0.89±0.12	−1.158	0.256
C to A	0.97±0.13	1.01±0.09	−1.221	0.231
C to B	1.03±0.08	1.02±0.09	0.221	0.827
C to D	0.98±0.15	0.99±0.10	−0.063	0.950
D to A	0.92±0.14	0.95±0.10	−0.754	0.456
D to B	0.94±0.13	0.95±0.08	−0.461	0.648
D to C	1.12±0.14	1.09±0.09	0.808	0.425

Note: Bold, p<0.05.
Abbreviations: Anti-LGI1-AE, anti-leucine-rich glioma-inactivated 1 antibody encephalitis.

statistically significant differences were observed between the two groups for other microstate transition probabilities (Table 2).

Brain Functional Network

The WPLI connectivity matrices for Microstate B and Microstate C in both the anti-LGI1-AE group and the control group are shown in Figures 2 and 3, respectively, with connection strength represented by color. In Microstate B, the patient group showed a significant increase in functional connectivity strength across the whole brain in the beta frequency band, with all *p*-values < 0.001. In Microstate C, the patient group exhibited enhanced delta-band global radial connectivity centered on the left occipital region (p = 0.002), and specific beta-band connectivity between the left posterior temporal region, midline structures, and the left parietal region (p = 0.037). The brain network connectivity maps are shown in Figure 4.

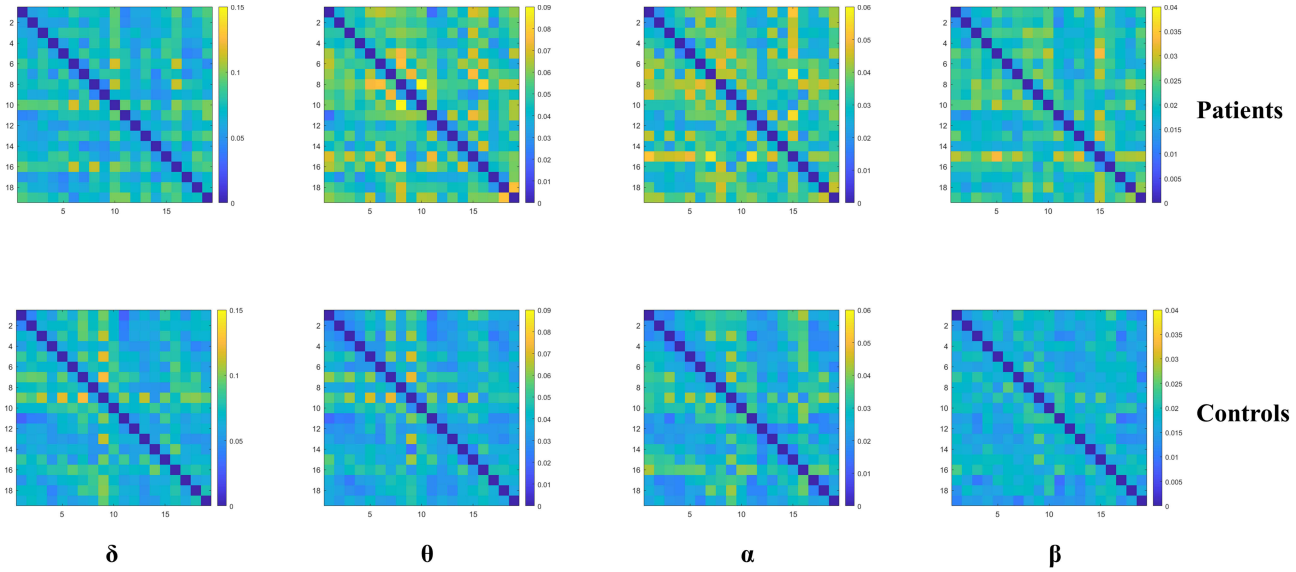

Figure 2 WPLI connectivity matrices for different frequency bands and electrode channels in microstate B for patients (top) and controls (bottom). The intensity of the colors reflects the magnitude of the WPLI values, frequency bands: δ (delta, 2–4 Hz), θ (theta, 4–8 Hz), α (alpha, 8–12 Hz), and β (beta, 12–20 Hz).

https://doi.org/10.2147/JIR.S540316

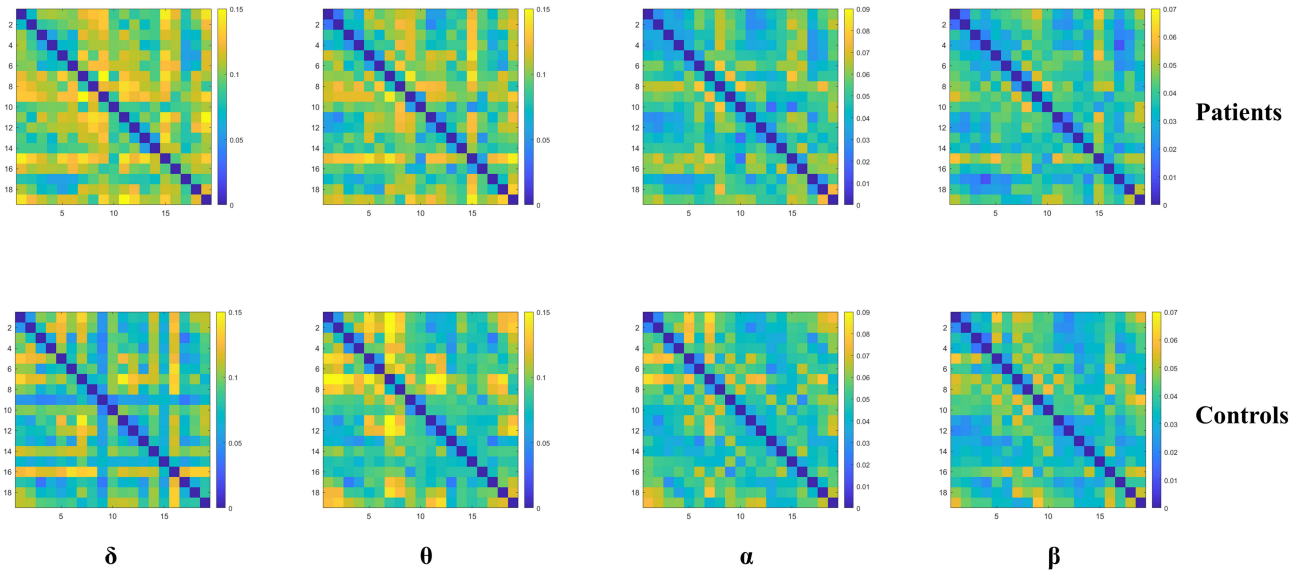

Figure 3 WPLI connectivity matrices for different frequency bands and electrode channels in microstate C for patients (top) and controls (bottom). The intensity of the colors reflects the magnitude of the WPLI values, frequency bands: δ (delta, 2–4 Hz), θ (theta, 4–8 Hz), α (alpha, 8–12 Hz), and β (beta, 12–20 Hz).

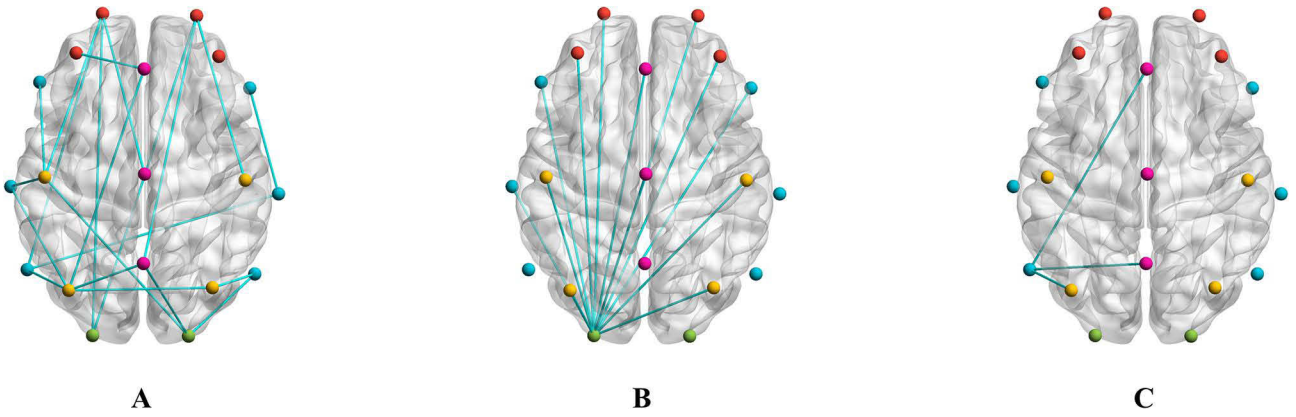

Figure 4 Functional connectivity analysis based on WPLI using a network-based approach. The images generated by BrainNet viewer show the significantly enhanced connectivity networks identified in the beta band of microstate B (**A**) and the delta (**B**) and beta (**C**) bands of microstate C.

Discussion

Unlike conventional approaches that construct functional brain networks by averaging phase-based connectivity indices, such as the WPLI, over extended EEG epochs, the present study estimated functional connectivity within distinct EEG microstates, which represent quasi-stable topographic patterns on the millisecond scale. This approach offers two key methodological advantages. First, it enables temporally resolved characterization of brain network reorganization, capturing rapid, state-dependent fluctuations that are otherwise obscured by global averaging. Second, because EEG microstates have been shown to correspond to canonical resting-state networks identified via fMRI, integrating WPLI with microstate segmentation provides a functionally meaningful framework for assessing frequency-specific connectivity alterations.

Our study reveals significant differences in the topographical distribution of Microstate A between the anti-LGI1-AE group and the control group. In the patient group, the frequency of Microstates B and C was significantly increased, while the Mean GFP of Microstate C was notably reduced. Functional network analysis based on the abnormal microstates showed that in Microstate B, the patients exhibited significantly enhanced whole-brain functional connectivity in the beta frequency band. In Microstate C, there was an increase in the whole-brain radiative connectivity in the

delta frequency band, with the left occipital region serving as the core. Furthermore, enhanced connectivity in the beta frequency band was observed between the left posterior temporal region, midline structures, and left parietal area. These findings provide new evidence for understanding the neurophysiological mechanisms underlying anti-LGI1-AE.

The topographical map of Microstate A showed significant differences between the anti-LGI1-AE group and the control group, indicating that the spatial patterns of EEG activity were altered in the encephalitis group. However, the overall microstate dynamics and the stability of its transitions remained relatively unchanged. Only minor trends were observed in local transition connections (A→B), which disappeared after FDR correction. This suggests that the abnormalities in microstate connectivity patterns induced by encephalitis may be subtle, or there may be insufficient statistical power to detect more substantial effects. Larger cohorts are needed to confirm these findings. Anti-LGI1-AE is a common form of limbic encephalitis,[10,37] and clinical MRI findings often show high signal abnormalities in the medial temporal lobe on T2/FLAIR sequences.[38] Britz et al[39] using simultaneous EEG-fMRI recordings, found that Microstate A is associated with negative BOLD signal activations in the bilateral superior temporal gyrus and middle temporal gyrus, areas related to auditory processing. Furthermore, Custo et al[40] through microstate source localization analysis in 164 subjects, identified that Microstate A is primarily localized in the left superior temporal gyrus, middle temporal gyrus, and left insula. Therefore, the changes observed in the topography of Microstate A in this study may reflect functional alterations associated with temporal lobe involvement, which is consistent with the clinical features of anti-LGI1-AE.

Britz et al[39] found that Microstate B was associated with negative BOLD signal activations in the bilateral secondary visual cortex (visual processing areas), while Microstate C was related to positive BOLD signal activations in the anterior cingulate cortex and bilateral inferior frontal gyrus. In further research by Custo et al[40] it was found that Microstate B was primarily localized in the bilateral occipital cortex (visual areas), while Microstate C was located in the precuneus and posterior cingulate cortex, which are core regions of the DMN. Additionally, some studies have found that Microstate C is positively correlated with levels of wakefulness, with higher coverage and occurrence frequency in states of high arousal.[41] In this study, the anti-LGI1-AE group showed significantly higher occurrences per second of Microstate B and C compared to the control group, and a significantly lower Mean GFP for Microstate C. However, no significant differences were found between the two groups in the topographical maps or other time parameters of Microstate B and C. These findings suggest that, in a resting state, the brain may be "over-utilizing" or "repeatedly entering" EEG patterns related to the visual network and DMN. This could reflect a compensatory regulatory mechanism or a pathological state of excessive activation, which may be associated with patients' cognitive and neurological deficits.

Our study identified enhanced brain connectivity in the beta frequency band in both Microstate B and C, and in the delta frequency band in Microstate C. Heine et al[14] found that in anti-LGI1-AE patients, there was significantly enhanced functional connectivity between the precuneus and other ventral DMN regions, as well as between the medial prefrontal cortex/anterior cingulate cortex and other dorsal DMN regions. This enhanced DMN connectivity was associated with improvements in memory. We hypothesize that these EEG microstate results may represent a compensatory regulatory mechanism, but they could also reflect pathological dysregulation of synchronization. Longitudinal studies tracking microstate dynamics and functional connectivity alongside clinical recovery and cognitive performance would help determine whether these network changes normalize with symptom improvement, indicating adaptive compensation, or persist and correlate with ongoing dysfunction, suggesting maladaptive pathology. Notably, the enhanced connectivity patterns observed in the anti-LGI1-AE group in the delta and beta frequency bands bear similarities to the electrophysiological patterns seen in anti-NMDA receptor encephalitis, which is characterized by excessive beta activity and widespread rhythmic delta activity.[42,43] This suggests that different autoimmune encephalitis disorders may share certain neurodynamic abnormalities within neural networks. These findings provide new insights into the common pathophysiological mechanisms of autoimmune encephalitis, although further multimodal imaging studies and longitudinal follow-up data are needed to validate these results.

This study is a retrospective analysis with a relatively small sample size, which may lead to insufficient statistical power, reducing the reliability and generalizability of the results. Additionally, the EEG recordings were made using the 10–20 system, which includes only 19 electrodes, limiting the spatial resolution and potentially affecting the accuracy of the study. It is important to note that this study focused solely on patients in the acute phase of anti-LGI1-

AE, while the pathophysiological mechanisms and clinical manifestations of the disease may dynamically change as the disease progresses. Therefore, the findings observed in the acute phase may not fully represent the entire disease course. To further validate the robustness of the results, future studies should be conducted with larger sample sizes, utilize high-density EEG or combine source localization techniques to improve spatial resolution, and employ a longitudinal design with 3–5 years of follow-up to dynamically observe the evolution of the disease. This would provide a more comprehensive understanding of the neurophysiological characteristics and long-term prognosis of anti-LGI1-AE.

Conclusion

This study found that patients with anti-LGI1-AE exhibited altered EEG microstate patterns and increased functional connectivity, particularly in the delta and beta frequency bands. These findings indicate that microstate-specific connectivity may represent a characteristic pattern of anti-LGI1-AE.

Abbreviations

Anti-LGI1-AE, Anti-leucine-rich glioma-inactivated 1 antibody encephalitis; CSF, Cerebrospinal fluid; DMN, Default mode networks; EEG, Electroencephalogram; FBDS, Faciobrachial dystonic seizures; FDR, False discovery rate; fMRI, Functional magnetic resonance imaging; FWER, Family-Wise Error Rate; GEV, Global explained variance; GFP, Global field power; LGI1, Leucine-rich glioma-inactivated 1; MRI, Magnetic resonance imaging; NBS, Network Based Statistic; WPLI, Weighted phase lag index.

Data Sharing Statement

The original contributions presented in the study are included in the article, further inquiries can be directed to Xiaoshan Wang.

Ethics Approval Statement

Our study was reviewed and approved by the ethical boards of the Affiliated Brain Hospital of Nanjing Medical University [Ethics Approval Number: 2025-KY046-02]. The informed consent process was implemented as follows: (1) All competent participants provided personally signed informed consent documents; (2) For patients lacking decision-making capacity due to impaired consciousness, cognitive deficits, or other neurological impairments, legally authorized representatives or court-appointed guardians executed the consent forms; (3) Posthumous data utilization required formal written authorization from next-of-kin. All consent documentation has been permanently archived in accordance with institutional data retention policies. All steps are in line with the Helsinki Declaration.

Author Contributions

All authors made a significant contribution to the work reported, whether that is in the conception, study design, execution, acquisition of data, analysis and interpretation, or in all these areas; took part in drafting, revising or critically reviewing the article; gave final approval of the version to be published; have agreed on the journal to which the article has been submitted; and agree to be accountable for all aspects of the work.

Funding

This work was supported by the National Natural Science Foundation of China [Grant No. 81471324], the General Project of the Nanjing Municipal Health Commission [Grant No. YKK21110], and the General Project of the Jiangsu Provincial Health Commission [Grant No. M2022065].

Disclosure

The authors declared no potential conflicts of interest with respect to the research, authorship, and/or publication of this article.

References

1. Uy CE, Binks S, Irani SR. Autoimmune encephalitis: clinical spectrum and management. *Pract Neurol*. 2021;21(5):412–423. doi:10.1136/practneurol-2020-002567
2. Flanagan EP, Kotsenas AL, Britton JW, et al. Basal ganglia T1 hyperintensity in LGI1-autoantibody faciobrachial dystonic seizures. *Neurol Neuroimmunol Neuroinflamm*. 2015;2(6):e161. doi:10.1212/nxi.0000000000000161
3. Gadoth A, Pittock SJ, Dubey D, et al. Expanded phenotypes and outcomes among 256 LGI1/CASPR2-IgG-positive patients. *Ann Neurol*. 2017;82(1):79–92. doi:10.1002/ana.24979
4. Binks SNM, Veldsman M, Easton A, et al. Residual fatigue and cognitive deficits in patients after leucine-rich glioma-inactivated 1 antibody encephalitis. *JAMA Neurol*. 2021;78(5):617–619. doi:10.1001/jamaneurol.2021.0477
5. Chan D, Henley SM, Rossor MN, Warrington EK. Extensive and temporally ungraded retrograde amnesia in encephalitis associated with antibodies to voltage-gated potassium channels. *Arch Neurol*. 2007;64(3):404–410. doi:10.1001/archneur.64.3.404
6. Butler CR, Miller TD, Kaur MS, et al. Persistent anterograde amnesia following limbic encephalitis associated with antibodies to the voltage-gated potassium channel complex. *J Neurol Neurosurg Psychiatry*. 2014;85(4):387–391. doi:10.1136/jnnp-2013-306724
7. Finke C, Prüss H, Heine J, et al. Evaluation of cognitive deficits and structural hippocampal damage in encephalitis with leucine-rich, glioma-inactivated 1 antibodies. *JAMA Neurol*. 2017;74(1):50–59. doi:10.1001/jamaneurol.2016.4226
8. Zhao Y, Yuan Y, Wang RZ, et al. Clinical, electroencephalogram and imaging characteristics of patients with anti-lgi1 antibody encephalitis: a multicenter cohort study. *CNS Neurosci Ther*. 2025;31(5):e70414. doi:10.1111/cns.70414
9. Almeida FC, Pereira AI, Mendes-Pinto C, et al. MR imaging findings in anti-leucine-rich glioma inactivated protein 1 encephalitis: a systematic review and meta-analysis. *AJNR Am J Neuroradiol*. 2024;45(7):977–986. doi:10.3174/ajnr.A8256
10. Graus F, Titulaer MJ, Balu R, et al. A clinical approach to diagnosis of autoimmune encephalitis. *Lancet Neurol*. 2016;15(4):391–404. doi:10.1016/s1474-4422(15)00401-9
11. Hébert J, Gros P, Lapointe S, et al. Searching for autoimmune encephalitis: beware of normal CSF. *J Neuroimmunol*. 2020;345:577285. doi:10.1016/j.jneuroim.2020.577285
12. Navarro V, Kas A, Apartis E, et al. Motor cortex and hippocampus are the two main cortical targets in LGI1-antibody encephalitis. *Brain*. 2016;139(Pt 4):1079–1093. doi:10.1093/brain/aww012
13. Liang M, Niu N, Jia C, et al. Diagnostic superiority of 18 F-FDG PET over MRI in detecting anti-LGI1 autoimmune encephalitis: a comparative study with insights into faciobrachial dystonic seizures mechanisms and recurrence identification. *Clin Nucl Med*. 2023;48(11):e516–e522. doi:10.1097/rlu.0000000000004862
14. Heine J, Prüss H, Kopp UA, et al. Beyond the limbic system: disruption and functional compensation of large-scale brain networks in patients with anti-LGI1 encephalitis. *J Neurol Neurosurg Psychiatry*. 2018;89(11):1191–1199. doi:10.1136/jnnp-2017-317780
15. Lehmann D, Ozaki H, Pal I. EEG alpha map series: brain micro-states by space-oriented adaptive segmentation. *Electroencephalogr Clin Neurophysiol*. 1987;67(3):271–288. doi:10.1016/0013-4694(87)90025-3
16. da Cruz JR, Favrod O, Roinishvili M, et al. EEG microstates are a candidate endophenotype for schizophrenia. *Nat Commun*. 2020;11(1):3089. doi:10.1038/s41467-020-16914-1
17. Khanna A, Pascual-Leone A, Michel CM, Farzan F. Microstates in resting-state EEG: current status and future directions. *Neurosci Biobehav Rev*. 2015;49:105–113. doi:10.1016/j.neubiorev.2014.12.010
18. Katayama H, Gianotti LR, Isotani T, et al. Classes of multichannel EEG microstates in light and deep hypnotic conditions. *Brain Topogr*. 2007;20(1):7–14. doi:10.1007/s10548-007-0024-3
19. Lehmann D, Pascual-Marqui RD, Strik WK, Koenig T. Core networks for visual-concrete and abstract thought content: a brain electric microstate analysis. *Neuroimage*. 2010;49(1):1073–1079. doi:10.1016/j.neuroimage.2009.07.054
20. Seitzman BA, Abell M, Bartley SC, Erickson MA, Bolbecker AR, Hetrick WP. Cognitive manipulation of brain electric microstates. *Neuroimage*. 2017;146:533–543. doi:10.1016/j.neuroimage.2016.10.002
21. Schiller B, Koenig T, Heinrichs M. Oxytocin modulates the temporal dynamics of resting EEG networks. *Sci Rep*. 2019;9(1):13418. doi:10.1038/s41598-019-49636-6
22. Nishida K, Morishima Y, Yoshimura M, et al. EEG microstates associated with salience and frontoparietal networks in frontotemporal dementia, schizophrenia and Alzheimer's disease. *Clin Neurophysiol*. 2013;124(6):1106–1114. doi:10.1016/j.clinph.2013.01.005
23. Zappasodi F, Croce P, Giordani A, et al. Prognostic value of EEG microstates in acute stroke. *Brain Topogr*. 2017;30(5):698–710. doi:10.1007/s10548-017-0572-0
24. V KR, Rajagopalan SS, Bhardwaj S, et al. Machine learning detects EEG microstate alterations in patients living with temporal lobe epilepsy. *Seizure*. 2018;61:8–13. doi:10.1016/j.seizure.2018.07.007
25. Fraschini M, Demuru M, Crobe A, Marrosu F, Stam CJ, Hillebrand A. The effect of epoch length on estimated EEG functional connectivity and brain network organisation. *J Neural Eng*. 2016;13(3):036015. doi:10.1088/1741-2560/13/3/036015
26. Ablin P, Cardoso JF, Gramfort A. Faster independent component analysis by preconditioning with hessian approximations. *IEEE Trans Signal Process*. 2018;66(15):4040–4049. doi:10.1109/TSP.2018.2844203
27. Pion-Tonachini L, Kreutz-Delgado K, Makeig S. ICLabel: an automated electroencephalographic independent component classifier, dataset, and website. *Neuroimage*. 2019;198:181–197. doi:10.1016/j.neuroimage.2019.05.026
28. Brunet D, Murray MM, Michel CM. Spatiotemporal analysis of multichannel EEG: CARTOOL. *Comput Intell Neurosci*. 2011;2011:813870. doi:10.1155/2011/813870
29. Férat V, Seeber M, Michel CM, Ros T. Beyond broadband: towards a spectral decomposition of electroencephalography microstates. *Hum Brain Mapp*. 2022;43(10):3047–3061. doi:10.1002/hbm.25834
30. Bagdasarov A, Roberts K, Bréchet L, Brunet D, Michel CM, Gaffrey MS. Spatiotemporal dynamics of EEG microstates in four- to eight-year-old children: age- and sex-related effects. *Dev Cogn Neurosci*. 2022;57:101134. doi:10.1016/j.dcn.2022.101134
31. Bréchet L, Brunet D, Birot G, Gruetter R, Michel CM, Jorge J. Capturing the spatiotemporal dynamics of self-generated, task-initiated thoughts with EEG and fMRI. *Neuroimage*. 2019;194:82–92. doi:10.1016/j.neuroimage.2019.03.029

32. Bagdasarov A, Brunet D, Michel CM, Gaffrey MS. Microstate analysis of continuous infant EEG: tutorial and reliability. *Brain Topogr*. 2024;37(4):496–513. doi:10.1007/s10548-024-01043-5
33. Vinck M, Oostenveld R, van Wingerden M, Battaglia F, Pennartz CM. An improved index of phase-synchronization for electrophysiological data in the presence of volume-conduction, noise and sample-size bias. *Neuroimage*. 2011;55(4):1548–1565. doi:10.1016/j.neuroimage.2011.01.055
34. Zalesky A, Fornito A, Bullmore ET. Network-based statistic: identifying differences in brain networks. *Neuroimage*. 2010;53(4):1197–1207. doi:10.1016/j.neuroimage.2010.06.041
35. Xia M, Wang J, He Y. BrainNet viewer: a network visualization tool for human brain connectomics. *PLoS One*. 2013;8(7):e68910. doi:10.1371/journal.pone.0068910
36. Tüzün E, Dalmau J. Limbic encephalitis and variants: classification, diagnosis and treatment. *Neurologist*. 2007;13(5):261–271. doi:10.1097/NRL.0b013e31813e34a5
37. Kelly MJ, Grant E, Murchison AG, et al. Magnetic resonance imaging characteristics of LGI1-antibody and CASPR2-antibody encephalitis. *JAMA Neurol*. 2024;81(5):525–533. doi:10.1001/jamaneurol.2024.0126
38. Britz J, Van De Ville D, Michel CM. BOLD correlates of EEG topography reveal rapid resting-state network dynamics. *Neuroimage*. 2010;52(4):1162–1170. doi:10.1016/j.neuroimage.2010.02.052
39. Custo A, Van De Ville D, Wells WM, Tomescu MI, Brunet D, Michel CM. Electroencephalographic resting-state networks: source localization of microstates. *Brain Connect*. 2017;7(10):671–682. doi:10.1089/brain.2016.0476
40. Hu W, Zhang Z, Zhao H, et al. EEG microstate correlates of emotion dynamics and stimulation content during video watching. *Cereb Cortex*. 2023;33(3):523–542. doi:10.1093/cercor/bhac082
41. Jeannin-Mayer S, André-Obadia N, Rosenberg S, et al. EEG analysis in anti-NMDA receptor encephalitis: description of typical patterns. *Clin Neurophysiol*. 2019;130(2):289–296. doi:10.1016/j.clinph.2018.10.017
42. Uchida Y, Kato D, Yamashita Y, Ozaki Y, Matsukawa N. Failure to improve after ovarian resection could be a marker of recurrent ovarian teratoma in anti-NMDAR encephalitis: a case report. *Neuropsychiatr Dis Treat*. 2018;14:339–342. doi:10.2147/ndt.S156603
43. Pascual-Marqui RD, Michel CM, Lehmann D. Segmentation of brain electrical activity into microstates: model estimation and validation. *IEEE Trans Biomed Eng*. 1995;42(7):658–665. doi:10.1109/10.391164